Feasibility of an alternative method to estimate glenohumeral joint center from videogrammetry measurements and CT/MRI of patients

Ehsan Sarshari[a,b], Matteo Mancuso[c], Alexandre Terrier[b], Alain Farron[d], Philippe Mullhaupt[a,*], Dominique Pioletti[b]

[a] *Automatic Control Laboratory, Ecole Polytechnique Fédérale de Lausanne (EPFL), Station 9, CH-1015 Lausanne, Switzerland*
[b] *Laboratory of Biomechanical Orthopedics, Ecole Polytechnique Fédérale de Lausanne (EPFL), Switzerland*
[c] *Laboratory of Movement Analysis and Measurement, Ecole Polytechnique Fédérale de Lausanne (EPFL), Switzerland*
[d] *Service of Orthopaedic Surgery and Traumatology, Lausanne University Hospital and University of Lausanne (CHUV), Switzerland*

Abstract

Videogrammetry is commonly used to record upper limb motions. However, it cannot track the glenohumeral joint center (GH). GH is required to reconstruct upper limb motions. Therefore, it is often estimated by separately measuring scapula motions using scapular kinematics measurements-devices (SKMD). Applications of SKMD are neither straightforward nor always noninvasive. Therefore, this work investigates the feasibility of an alternative method to estimate GH from videogrammetry using a CT/MRI image of subject's glenohumeral joint and without requiring SKMD. In order to evaluate the method's accuracy, its GH estimations were compared to reference GH trajectories. The method was also applied to estimate scapula configurations and reconstruct an abduction motion measured by videogrammetry. The accuracy of GH estimations were within 5 mm, and the reconstructed motion was in excellent agreement with reported *in vivo* measurements.

Keywords: upper limb kinematics, glenohumeral joint center, videogrammetry, multi-segment optimization, scapular kinematics

1. Introduction

Videogrammetry tracks trajectories of skin-fixed markers placed on palpable bony landmarks [49]. It is not possible to palpate and measure GH using

*Corresponding author.
Email address: philippe.muellhaupt@epfl.ch (Philippe Mullhaupt)

videogrammetry. However, GH is required to reconstruct upper limb motions [27, 37].

Several methods have been developed to estimate GH, namely: formal [5, 12, 15, 17, 40, 50] and predictive methods [6, 26, 33, 39]. Formal methods estimate GH by finding either the closest point to all humerus instantaneous helical axes [5, 12, 40, 50] or the center of a sphere passing through humerus markers [15, 17]. Predictive methods estimate GH either through regressive equations between scapula markers and GH [6, 26, 33] or generic offsets from scapula markers [6, 39]. Formal methods estimate GH more accurately and are preferred over predictive methods whose accuracy drops significantly during arm motions [6, 12]. However, the main limitation of formal methods is their dependency on SKMD.

Due to soft tissue artifacts only two landmarks, angulus acromialis (AA) and acromioclavicular (AC), of the scapula can be practically tracked by videogrammetry [24, 31]. SKMD is therefore used to measure scapula motions. Several SKMD have been proposed, including intracortical bone-fixed pins [22], regressive equations [8–10, 16, 18, 19], scapula locator fixtures [32, 36], and acromion markers-tree [45]. However, applications of SKMD are neither straightforward nor always non-invasive.

Therefore, this study aims at investigating the feasibility of an alternative method to estimate GH from videogrammetry using a CT/MRI of subject's glenohumeral joint and without requiring SKMD. Provided GH estimations, trigonum scapulae (TS) and angulus inferior (AI) of scapula are consequently estimated defining the scapula configurations. The method's accuracy is evaluated by comparing its GH estimations to reference GH trajectories. The method is then applied to reconstruct an abduction motion measured by videogrammetry and compare the reconstructed motion to reported *in vivo* measurements.

2. Methods

2.1. Kinematic model

A kinematic model of the upper limb is developed from MRI scans (T1-weighted sequences, 3-T, 0.9 mm isotropic spatial resolution) of the hemi-thorax of a healthy male subject (29 year, 186 cm, 85.5 Kg) (Fig. 1a). It consists of six rigid bodies: thorax, clavicle, scapula, humerus, ulna, and radius (rigidly tied with hand). It has five joints, including three ball-and-socket joints for sternoclavicular (SC), acromioclavicular (AC), and glenohumeral (GH) joints and two hinge joints for humeroulnar (HU) and radioulnar (RU) joints (Fig. 1b,c). Two holonomic constraints restrict TS and AI to glide over ribcage. This results in nine degrees of freedom. Fourteen bony landmarks are identified from the MRI scans to define bone-fixed frames and joints coordinates following ISB recommendations [51]. The landmarks are: incisura jugularis (IJ), processus xiphoideus (PX), 7th cervical vertebra (C7), 8th thoracic vertebra (T8), SC, AC, AA, TS, AI, GH, humerus medial epicondyle (EM), humerus lateral epicondyle (EL), radial styloid (RS), and ulnar styloid (US). Given that the GH is not a

bony landmark, its position is defined as the center of a sphere fitting the glenoid fossa [47]. To this end, a MATLAB (The MathWorks, Natick, MA, USA) routine [44] is used to fit a sphere on the fossa surface obtained by segmentation of MRI in Amira (FEI Visualization Sciences Group,Bordeaux, France). Thorax is the inertial frame. Eleven generalized coordinates ($\boldsymbol{q} = [q_1 \ \dots \ q_{11}]^T$) are considered to uniquely define each joint configuration. Forward kinematic map (ξ) of the kinematic model defines inertial coordinates of the j^{th} landmark ($\boldsymbol{x}_j$) for given joint configurations (Eq. 1).

$$\begin{aligned} &\xi : C_s \subset R^{11} \mapsto W_s \subset R^3 \\ &\xi(\boldsymbol{q}(t)) = \boldsymbol{x}_j(t), \quad j = \{\text{C7}, \ \dots, \ \text{RS}\}_{1\times 14} \\ &\Phi_{\text{TS}}(\boldsymbol{q}(t)) = 0 \\ &\Phi_{\text{AI}}(\boldsymbol{q}(t)) = 0 \end{aligned} \tag{1}$$

Where, C_s and W_s are coordinate and work spaces [42]. The holonomic constraints ($\Phi_{\text{TS}} = 0$ and $\Phi_{\text{AI}} = 0$) represent kinematic relationships between scapula and thorax (Eq. 2). The constraints restrict TS and AI to always lie on two different ellipsoids approximating ribcage and the underlying soft tissues of each one of TS and AI.

$$\begin{aligned} \Phi_{\text{TS}}(\boldsymbol{q}(t)) &= ({}_t\boldsymbol{TS}(t) - {}_t\boldsymbol{e}_0)^T E_{\text{TS}}({}_t\boldsymbol{TS}(t) - {}_t\boldsymbol{e}_0) - 1 = 0 \\ \Phi_{\text{AI}}(\boldsymbol{q}(t)) &= ({}_t\boldsymbol{AI}(t) - {}_t\boldsymbol{e}_0)^T E_{\text{AI}}({}_t\boldsymbol{AI}(t) - {}_t\boldsymbol{e}_0) - 1 = 0 \end{aligned} \tag{2}$$

Where, the left-hand side subscript t denotes that the landmarks are in thorax frame. The centers of the two ellipsoids coincide and are at ${}_t\boldsymbol{e}_0$. A single ellipsoid centered at ${}_t\boldsymbol{e}_0$ is first fitted to the ribcage. Then, starting from this ellipsoid, adjustments are made to fit one ellipsoid to AI and another ellipsoid to TS. The ellipsoids including TS and AI have matrices E_{TS} and E_{AI}, respectively [25].

2.2. Estimation of GH

Ball-and-socket approximation of the glenohumeral joint implies that GH is a point shared between scapula and humerus (Fig. 2). Therefore, its positions as a point either on scapula or humerus should result in the same point in thorax frame (${}_t\mathbf{GH}$). This can be concisely written as

$$\underbrace{{}^t_hR(\alpha)\ {}_h\mathbf{GH} + {}_t\mathbf{EM}}_{{}_t\mathbf{GH} \text{ as a point on humerus}} = \underbrace{{}^t_sR(\beta)\ {}_s\mathbf{GH} + {}_t\mathbf{AC}}_{{}_t\mathbf{GH} \text{ as a point on scapula}} \tag{3}$$

Where, ${}^t_hR(\alpha)$ and ${}^t_sR(\beta)$ are rotation matrices from humerus and scapula frames to thorax frame defined in Eq. 4 using Rodrigues' rotation formula [1]. The left-hand side subscripts h and s specify that the landmarks are in humerus and scapula frames, respectively. Constants ${}_h\mathbf{GH}$ and ${}_s\mathbf{GH}$ are obtained from subject's CT/MRI. From a CT of the subject to be studied ${}_{\text{CT}}\mathbf{GH}$, ${}_{\text{CT}}\mathbf{EM}$, ${}_{\text{CT}}\mathbf{EL}$ that are the landmarks in the CT or MRI coordinate system can be obtained for a single arm configuration. Then, ${}_{\text{h}}\mathbf{GH}$ is defined as ${}_{\text{h}}\mathbf{GH} = {}^h_{\text{CT}}R\ {}_{\text{CT}}\mathbf{GH}$. The rotation matrix ${}^h_{\text{CT}}R$ from the CT or MRI coordinate system to the humeral

coordinate system is obtained following the ISB recommendations [51]. Similarly, ${}_s\mathbf{GH}$ is obtained as ${}_s\mathbf{GH} = {}^s_{\mathrm{CT}}R\ ({}_{\mathrm{CT}}\mathbf{GH} - {}_{\mathrm{CT}}\mathbf{AC})$. The rotation matrix ${}^s_{\mathrm{CT}}R$ from the CT or MRI coordinate system to the scapula coordinate system is obtained following the ISB recommendations.

$$\begin{aligned} {}^t_h R(\alpha) &= \boldsymbol{d}_h {\boldsymbol{d}_h}^T + \cos\alpha(I - \boldsymbol{d}_h {\boldsymbol{d}_h}^T) + \sin\alpha[\boldsymbol{d}_h] \\ {}^t_s R(\beta) &= \boldsymbol{d}_s {\boldsymbol{d}_s}^T + \cos\beta(I - \boldsymbol{d}_s {\boldsymbol{d}_s}^T) + \sin\beta[\boldsymbol{d}_s] \end{aligned} \tag{4}$$

Where, $\boldsymbol{d}_h = {}_t\mathbf{EM} - {}_t\mathbf{EL}$ and $\boldsymbol{d}_s = {}_t\mathbf{AC} - {}_t\mathbf{AA}$, and α and β are unknown rotation angles of humerus and scapula around $\boldsymbol{d}_h$ and $\boldsymbol{d}_s$. The cross product matrices of $\boldsymbol{d}_h$ and $\boldsymbol{d}_s$ are denoted by $[\boldsymbol{d}_h]$ and $[\boldsymbol{d}_s]$, respectively.

Equation 3 can be solved for α and β for each frame of measurements using nonlinear root-search methods (e.g. Matlab `fminsearch`). The resulting α and β provide two estimations for GH in thorax frame (${}_t\mathbf{GH}$). Given that the measured positions of AC, AA, EM, and EL are subject to soft-tissue artifacts, the resulting two estimations of ${}_t\mathbf{GH}$ might come apart. Therefore, the following optimization is casted to minimize the distance between the resulting two estimations by compensating effects of soft-tissue artifacts on EM and EL.

$$\begin{aligned} \min_{\boldsymbol{\mu}} .\quad & \left({}_t\mathbf{GH}_{e_h}(\alpha, \boldsymbol{\mu}) - {}_t\mathbf{GH}_{e_s}(\beta)\right)^2 \\ \text{s.t.}\quad & |\boldsymbol{\mu}| \leq C \end{aligned} \tag{5}$$

Where, ${}_t\mathbf{GH}_{e_h}$ and ${}_t\mathbf{GH}_{e_s}$ are the resulting estimations obtained through humerus and scapula frames, respectively. The decision variable $\boldsymbol{\mu}$ is a 3×1 vector added to $\boldsymbol{d}_h$ to compensate soft-tissue artifacts. It is bounded by C to vary according to reported values for EM and EL soft-tissue artifacts ($C = 3$ cm [23]).

Estimated GH together with measured AC and AA provide three points on scapula. Therefore, TS and AI are readily estimated, given that they also belong to the same bone segment. The resulting GH, TS, and AI estimations are used in Section 2.3 to reconstruct the shoulder kinematics including scapula configuration.

It is worth noting that Eq. 3 has an intuitive geometrical interpretation. In fact, it estimates GH by intersecting four spheres centered at AC, AA, EM, and EL. Their radii can be defined from a single CT/MRI scan of the glenohumeral joint of the subject to be studied. This intersection can be defined using the intersection theory of quadric surfaces [25].

2.3. Multi-segment optimization

Multi-segment optimization finds joint angles ($\boldsymbol{q}_i$) for each frame of measurements (i) such that the overall distance between the measured markers ($\boldsymbol{x}_{e_j}$) and their associating landmarks ($\boldsymbol{x}_{m_j}$) is minimized, while satisfying the forward kinematics map (Eq. 6). Estimations of GH, TS, and AI are considered

on behalf of their missing measured trajectories.

$$\begin{aligned} \min_{\boldsymbol{q}_i} . \quad & \textstyle\sum_j (\boldsymbol{x}_{m_{j,i}}(\boldsymbol{q}_i) - \boldsymbol{x}_{e_{j,i}})^T W (\boldsymbol{x}_{m_{j,i}}(\boldsymbol{q}_i) - \boldsymbol{x}_{e_{j,i}}) \\ \text{s.t.} \quad & \Phi_{\text{TS}}(\boldsymbol{q}_i) = 0 \\ & \Phi_{\text{AI}}(\boldsymbol{q}_i) = 0 \end{aligned} \tag{6}$$

Where, $j = \{\text{C7}, \ \ldots, \ \text{RS}\}_{1\times 14}$, and W is a positive definite weighting-matrix that can be used to account for different amount of soft-tissue artifacts occur at each marker [2]. For simplicity, W is set to the identity matrix here. This optimization is a nonlinear programming problem [4] that can be solved using iterative methods e.g. Matlab `fmincon`.

2.4. Accuracy

A numerical method [21], called minimal coordinates approach, is used to virtually generate trajectories for all fourteen model's landmarks during forward flexion. The minimal coordinates approach is indeed the only available method that can plan the upper limb motions from a limited measurement data [21]. In the minimal coordinates approach, the shoulder girdle contact constraint is replaced by a novel parallel mechanism that results in a minimal set of generalized coordinates. The resulting minimal coordinates are independent and considerably simplify motion planning. The accuracy of the minimal coordinates approach has been already investigated in [20] against *in vivo* measurements of [13]. An arm motion from the arm neutral position to 150° flexion is simulated using the minimal coordinates approach. To this end, the scapular minimal coordinates corresponding to beginning and end of the motion are chosen as per [20] such that the model bony landmarks match the bony landmarks reported ~~in~~ [13] ~~for only~~ beginning and end of the motion. Until 30° arm elevation, the scapular minimal coordinates are ~~kept constant at the values for the beginning~~ and ~~then are varied with a linear function of time until end of the motion~~. The definition of the arm minimal coordinates are trivial using a linear function of time until 150° flexion. Eventually, GH of the virtually generated trajectories is considered as the reference GH (${}_t\boldsymbol{GH}_r$). Soft-tissue artifacts are numerically produced and added to the trajectories. Soft-tissue artifacts are defined according to [7, 43] as $a \sin \omega t + \phi$, where a lies between 1 cm to 3 cm, and ω and ϕ are smaller than 4 Hz and 2π, respectively. The resulting trajectories are considered as pseudo-measurements. The method is used to estimate GH from the pseudo-measurements.

The accuracy results are presented in terms of the distance d between estimated GH (${}_t\boldsymbol{GH}_e$) and ${}_t\boldsymbol{GH}_r$ for each frame of data.

2.5. Motion reconstruction from videogrammetry

Eleven bony landmarks are palpated using skin-fixed markers on the same subject, including IJ, PX, C7, T8, SC, AC, AA, EM, EL, RS, and US (Fig. 1d). The markers trajectories are recorded for 10 trials using an 8-camera VICON videogrammetry at 100 Hz, while the subject is performing an abduction motion

in scapula plane with a fully extended forearm. The recorded data of each trial is low-passed filtered [49]. Then, means and standard deviations (σ) of the filtered trajectories for the 10 trials are obtained.

The method is used to estimate GH and consequently TS and AI. Then, multi-segment optimization is used to reconstruct the motion in terms of the joints angles. Sensitivity of the joints angles ($\boldsymbol{q}(\Delta\boldsymbol{x})$) to markers variations around their means ($\Delta\boldsymbol{x}$) are also approximated by a first order approximation (Eq. 7) [14].

$$\boldsymbol{q}(\Delta\boldsymbol{x}) = \boldsymbol{q}^{\star} + M^{-1}N\Delta\boldsymbol{x} + O(|\Delta\boldsymbol{x}|) \tag{7}$$

Where, $\boldsymbol{q}^{\star}$ is solution of the multi-segment optimization associated with measurements means. The matrices M and N are defined as follows.

$$M = \begin{bmatrix} \nabla^2 L & \nabla\Phi_{\mathrm{TS}} & \nabla\Phi_{\mathrm{AI}} \\ \nabla\Phi_{\mathrm{TS}} & 0 & 0 \\ \nabla\Phi_{\mathrm{AI}} & 0 & 0 \end{bmatrix} \quad , \quad N = \begin{bmatrix} -\frac{\partial}{\partial\Delta\boldsymbol{x}}(\nabla L) & -\frac{\partial\Phi_{\mathrm{TS}}}{\partial\Delta\boldsymbol{x}} & -\frac{\partial\Phi_{\mathrm{AI}}}{\partial\Delta\boldsymbol{x}} \end{bmatrix}^T \tag{8}$$

Where, L is Lagrangian of the multi-segment optimization (Eq. 6).

The results consist of eleven joints angles, including axial rotation, depression/elevation, protraction/retraction of SC, posterior/anterior tilt, downward/upward rotation, protraction/retroaction of AC, axial rotation, adduction/abduction, flexion/extension of GH, extension/flexion of HU, and pronation/supination of RU joints. Joints angles are presented in thorax frame along arm abduction angle, except for HU and RU joints, which are given with respect to their proximal joints. Angles sensitivities to $\pm 1\sigma$ markers variations are also illustrated.

3. Results

3.1. Accuracy

The distance d was less than 1 mm until 20% of arm flexion and reached 5 mm at 60% of the movement (Fig. 3).

3.2. Motion reconstruction from videogrammetry

Clavicular elevation and retraction increased by 16° and 26° during arm elevation, despite its axial rotation, and were equally (about 13°) affected by landmarks variations (Fig. 4).

Scapular posterior tilt increased by 5° from an anteriorly tilted configuration. Scapular upward rotation increased from a neutral position to 30°. Scapular protraction decreased by 7°. The landmarks variations affected posterior/anterior tilt by 5°, downward/upward rotation by 13°, and protraction/retraction by 6°.

Humerus rotated externally by 49° from an internally orientated position. Abduction increased by 68°, and flexion increased by 30°. Axial rotation and adduction/abduction were almost 250% more sensitive to landmarks variations than flexion/extension angle.

Forearm flexed 6° from full extension, and RU supination increased by 9° (palm of the hand faced anteriorly). Compared to other joint angles, forearm illustrated the highest sensitivities to landmarks variations: (17° and 22° for HU and RU joints, respectively).

4. Discussion

The aim of this study was to develop a method to estimate GH from videogrammetry using a CT/MRI of subject's glenohumeral joint and without requiring SKMD. The method accuracy was verified, and the method was applied to reconstruct a videogrammetry-based measured motion.

The accuracy decreased towards the end of motion that could be associated with increase in the simulated soft-tissue artifacts. The increasing trend considered for soft-tissue artifacts was consistent with previous *in vivo* observations [7, 43]. Compared to the application of a reported predictive method [6] on the same pseudo-measurements, GH estimation was improved around 85% with our method. The choice of the predictive method [6] among the available predictive methods in the literature could be justified by the following main reasons. First, contrary to most of the predictive methods [33, 51], it did not require trajectories of TS or AI. Trajectories of TS and AI could be only either measured using SKMD or estimated based on GH trajectories. Second, it was indeed among the few predictive methods whose accuracy and inter-individual reliability have been assessed against other established predictive methods [26, 33, 39, 51] as well as *in vivo* GH measurements.

Application of the method to videogrammetry measurements followed by multi-segment optimization provided joint angles that were consistent with reported *in vivo* [28, 48] and numerical studies [34, 41].

Clavicular axial rotation was overlooked in our motion reconstruction, whereas several *in vivo* studies reported 0° to 30° variations [28, 38]. Clavicular axial rotation could be enforced using an extra constraint on q_1 in Eq. 6 [46]. However, given few weak muscles attached to the clavicle, underestimating its axial rotation could only have negligible effects on musculoskeletal models outcomes [35].

AC joint angles were in good agreement with *in vivo* measurements [28, 48]. Normalized root mean square error (NRMSE) [30] between the estimated scapular posterior/anterior tilt and the measurements of [48] and [28] were 0.99 and 0.91, respectively. The NRMSE between the estimated scapular downward/upward rotation and the measurements was consistent with the results of [48] (NRMSE above 0.77). The zero downward rotation estimated by our model placed scapula in a rest position for the beginning of motion and was commonly reported [29, 34], although the angle reported in [28] was −16°. Estimated scapular protraction/retraction was consistent with both *in vivo* measurements of [28, 48] (NRMSE above 0.81).

The forearm joint angles had the highest sensitivities to variations in markers trajectories. This could be explained by propagation of the errors introduced through proximal bone segments. The sensitivity analysis investigated

the sensitivity of the resulting joint angles to the recorded variations in markers trajectories. Although this provided valuable information about the reliability of the resulting joint angles, a more detailed sensitivity study was required to investigate influences of positioning each individual marker. Provided this, special attention could be paid to more robustly capture the trajectories of the influential markers.

The effects of soft-tissue artifacts on GH estimations were compensated by an optimization. The optimization accounted for merely EM and EL soft-tissue artifacts, since AC and AA were subject to relatively negligible amount of soft-tissue artifacts [3, 11, 34]. In addition, from a mathematical point of view, it was possible to introduce a second decision variable into the optimization for AC and AA soft-tissue artifacts. However, this could result in an indeterminate optimization with infinite solutions. In order to uniquely solve this indeterminate optimization, complementary information on the ratio of EM-EL to AC-AA soft-tissue artifacts was required. Application of a cluster attached to the humerus could potentially reduce the amount of soft-tissue artifacts, requiring less correction from the optimization.

A major limitation of this study was that only one subject was recorded. More subjects could allow a better evaluation of the method, specially its performance in dealing with inter-individual differences. Given that the method required a CT/MRI scan of the subject's glenohumeral joint, it could be expected that the method inherently considered inter-individual differences. Another limitation was the dependency of the method on subject's CT/MRI. The CT/MRI is often performed during subjects' routine clinical examinations. Therefore, it would not widely affect practical applications of the method for subject-specific modeling. Another potential limitation of the method could be due to the high error sensitivity of the direction connecting EL and EM and/or AC and AA, given the short distances between them. Therefore, special care was taken in this study in placing the markers on these bony landmarks. In addition, an additional marker on the Capitulum would help in compensating the error in direction connecting EL and EM.

The resulting GH estimations and scapula kinematics were compared to those of a commonly used predictive method and *in vivo* measurements, respectively. These partially confirmed the feasibility of the present method as an alternative approach to estimate the GH and scapula kinematics without SKMD. Indeed, direct comparisons of the method estimations with measurements from SKMD such as scapula locator and acromion cluster could enrich the confidence into the method estimations.

In conclusion, the method provided estimations for GH, TS, and AI with sufficient accuracy using a CT/MRI scan of subject's glenohumeral joint and without requiring SKMD. Provided GH, TS, and AI estimations, a videogrammetry-based measured motion was reconstructed using multi-segment optimization which resulted in scapula configurations that were in good agreement with reported *in vivo* measurements. The developed method ~~would~~ be used to retrospectively study kinematics of ~~a cohort of~~ patients using a scaled-generic shoulder musculoskeletal model. A generic motion data ~~would~~ be scaled to each ~~one~~

~~of the~~ patient~~s~~ whose CT/MRI ~~were~~ available as a part of the~~ir~~ routine clinical examination. ~~In such retrospective studies that access to the patients and performing patient specific kinematic measurements with SKMD could face difficulties, the developed method would be considered as an alternative solution, despite its limitations.~~

Acknowledgment

This project was supported by the Swiss National Science Foundation [143704].

References

[1] Baruh, H., 1999. Analytical dynamics. WCB/McGraw-Hill Boston.

[2] Begon, M., Dal Maso, F., Arndt, A., Monnet, T., 2015. Can optimal marker weightings improve thoracohumeral kinematics accuracy? Journal of biomechanics 48 (10), 2019–2025.

[3] Blache, Y., Dumas, R., Lundberg, A., Begon, M., 2017. Main component of soft tissue artifact of the upper-limbs with respect to different functional, daily life and sports movements. Journal of biomechanics 62, 39–46.

[4] Boyd, S., Vandenberghe, L., 2004. Convex optimization. Cambridge university press.

[5] Camomilla, V., Cereatti, A., Vannozzi, G., Cappozzo, A., 2006. An optimized protocol for hip joint centre determination using the functional method. Journal of biomechanics 39 (6), 1096–1106.

[6] Campbell, A., Lloyd, D., Alderson, J., Elliott, B., 2009. Mri development and validation of two new predictive methods of glenohumeral joint centre location identification and comparison with established techniques. Journal of biomechanics 42 (10), 1527–1532.

[7] Cheze, L., Fregly, B., Dimnet, J., 1995. A solidification procedure to facilitate kinematic analyses based on video system data. Journal of biomechanics 28 (7), 879–884.

[8] De Groot, J., Brand, R., 2001. A three-dimensional regression model of the shoulder rhythm. Clinical Biomechanics 16 (9), 735–743.

[9] de Groot, J. H., Valstar, E. R., Arwert, H. J., 1998. Velocity effects on the scapulo-humeral rhythm. Clinical Biomechanics 13 (8), 593–602.

[10] Dickerson, C. R., Chaffin, D. B., Hughes, R. E., 2007. A mathematical musculoskeletal shoulder model for proactive ergonomic analysis. Computer methods in biomechanics and biomedical engineering 10 (6), 389–400.

[11] Duprey, S., Naaim, A., Moissenet, F., Begon, M., Chèze, L., 2017. Kinematic models of the upper limb joints for multibody kinematics optimisation: An overview. Journal of biomechanics 62, 87–94.

[12] Ehrig, R. M., Taylor, W. R., Duda, G. N., Heller, M. O., 2006. A survey of formal methods for determining the centre of rotation of ball joints. Journal of biomechanics 39 (15), 2798–2809.

[13] El Habachi, A., Duprey, S., Cheze, L., Dumas, R., 2015. A parallel mechanism of the shoulder—application to multi-body optimisation. Multibody System Dynamics 33 (4), 439–451.

[14] Fiacco, A. V., 1976. Sensitivity analysis for nonlinear programming using penalty methods. Mathematical programming 10 (1), 287–311.

[15] Gamage, S. S. H. U., Lasenby, J., 2002. New least squares solutions for estimating the average centre of rotation and the axis of rotation. Journal of biomechanics 35 (1), 87–93.

[16] Grewal, T.-J., Dickerson, C. R., 2013. A novel three-dimensional shoulder rhythm definition that includes overhead and axially rotated humeral postures. Journal of biomechanics 46 (3), 608–611.

[17] Halvorsen, K., 2003. Bias compensated least squares estimate of the center of rotation. Journal of Biomechanics 36 (7), 999–1008.

[18] Högfors, C., Peterson, B., Sigholm, G., Herberts, P., 1991. Biomechanical model of the human shoulder joint—ii. the shoulder rhythm. Journal of biomechanics 24 (8), 699–709.

[19] Holzbaur, K. R., Murray, W. M., Delp, S. L., 2005. A model of the upper extremity for simulating musculoskeletal surgery and analyzing neuromuscular control. Annals of biomedical engineering 33 (6), 829–840.

[20] Ingram, D., 2015. Musculoskeletal model of the human shoulder for joint force estimation.

[21] Ingram, D., Engelhardt, C., Farron, A., Terrier, A., Müllhaupt, P., 2016. Modelling of the human shoulder as a parallel mechanism without constraints. Mechanism and Machine Theory 100, 120–137.

[22] Karduna, A. R., McClure, P. W., Michener, L. A., Sennett, B., 2001. Dynamic measurements of three-dimensional scapular kinematics: a validation study. Journal of biomechanical engineering 123 (2), 184–190.

[23] Klopčar, N., Lenarčič, J., 2006. Bilateral and unilateral shoulder girdle kinematics during humeral elevation. Clinical Biomechanics 21, S20–S26.

[24] Lempereur, M., Brochard, S., Burdin, V., Rémy-Néris, O., 2010. Difference between palpation and optoelectronics recording of scapular motion. Computer methods in biomechanics and biomedical engineering 13 (1), 49–57.

[25] Levin, J. Z., 1979. Mathematical models for determining the intersections of quadric surfaces. Computer Graphics and Image Processing 11 (1), 73–87.

[26] Lloyd, D., Alderson, J., Elliott, B., 2000. An upper limb kinematic model for the examination of cricket bowling: A case study of mutiah muralitharan. Journal of sports sciences 18 (12), 975–982.

[27] Lu, T.-W., O'connor, J., 1999. Bone position estimation from skin marker coordinates using global optimisation with joint constraints. Journal of biomechanics 32 (2), 129–134.

[28] Ludewig, P. M., Phadke, V., Braman, J. P., Hassett, D. R., Cieminski, C. J., LaPrade, R. F., 2009. Motion of the shoulder complex during multiplanar humeral elevation. The Journal of Bone and Joint Surgery. American volume. 91 (2), 378.

[29] MacLean, K. F., Chopp, J. N., Grewal, T.-J., Picco, B. R., Dickerson, C. R., 2014. Three-dimensional comparison of static and dynamic scapular motion tracking techniques. Journal of Electromyography and Kinesiology 24 (1), 65–71.

[30] MatlabDocumentation, 2012. Goodness of fit between test and reference data. URL https://ch.mathworks.com/help/ident/ref/goodnessoffit.html

[31] Matsui, K., Shimada, K., Andrew, P. D., 2006. Deviation of skin marker from bone target during movement of the scapula. Journal of Orthopaedic Science 11 (2), 180–184.

[32] McQuade, K. J., Smidt, G. L., 1998. Dynamic scapulohumeral rhythm: the effects of external resistance during elevation of the arm in the scapular plane. Journal of Orthopaedic & Sports Physical Therapy 27 (2), 125–133.

[33] Meskers, C., Van der Helm, F. C., Rozendaal, L., Rozing, P., 1997. In vivo estimation of the glenohumeral joint rotation center from scapular bony landmarks by linear regression. Journal of biomechanics 31 (1), 93–96.

[34] Naaim, A., Moissenet, F., Duprey, S., Begon, M., Cheze, L., 2017. Effect of various upper limb multibody models on soft tissue artefact correction: A case study. Journal of biomechanics 62, 102–109.

[35] Prinold, J. A., Masjedi, M., Johnson, G. R., Bull, A. M., 2013. Musculoskeletal shoulder models: a technical review and proposals for research foci. Proceedings of the Institution of Mechanical Engineers, Part H: Journal of Engineering in Medicine 227 (10), 1041–1057.

[36] Prinold, J. A., Shaheen, A. F., Bull, A. M., 2011. Skin-fixed scapula trackers: a comparison of two dynamic methods across a range of calibration positions. Journal of biomechanics 44 (10), 2004–2007.

[37] Roux, E., Bouilland, S., Godillon-Maquinghen, A.-P., Bouttens, D., 2002. Evaluation of the global optimisation method within the upper limb kinematics analysis. Journal of biomechanics 35 (9), 1279–1283.

[38] Sahara, W., Sugamoto, K., Murai, M., Tanaka, H., Yoshikawa, H., 2007. The three-dimensional motions of glenohumeral joint under semi-loaded condition during arm abduction using vertically open mri. Clinical Biomechanics 22 (3), 304–312.

[39] Schmidt, R., Disselhorst-Klug, C., Silny, J., Rau, G., 1999. A marker-based measurement procedure for unconstrained wrist and elbow motions. Journal of Biomechanics 32 (6), 615–621.

[40] Schwartz, M. H., Rozumalski, A., 2005. A new method for estimating joint parameters from motion data. Journal of biomechanics 38 (1), 107–116.

[41] Seth, A., Matias, R., Veloso, A. P., Delp, S. L., 2016. A biomechanical model of the scapulothoracic joint to accurately capture scapular kinematics during shoulder movements. PloS one 11 (1), e0141028.

[42] Siciliano, B., Khatib, O., 2008. Springer handbook of robotics. Springer Science & Business Media.

[43] Taylor, W. R., Ehrig, R. M., Duda, G. N., Schell, H., Seebeck, P., Heller, M. O., 2005. On the influence of soft tissue coverage in the determination of bone kinematics using skin markers. Journal of Orthopaedic Research 23 (4), 726–734.

[44] Terrier, A., Ston, J., Larrea, X., Farron, A., 2014. Measurements of three-dimensional glenoid erosion when planning the prosthetic replacement of osteoarthritic shoulders. The bone & joint journal 96 (4), 513–518.

[45] van Andel, C., van Hutten, K., Eversdijk, M., Veeger, D., Harlaar, J., 2009. Recording scapular motion using an acromion marker cluster. Gait & posture 29 (1), 123–128.

[46] van der Helm, F. C., Pronk, G. M., 1995. Three-dimensional recording and description of motions of the shoulder mechanism. Journal of biomechanical engineering 117 (1), 27–40.

[47] Veeger, H., 2000. The position of the rotation center of the glenohumeral joint. Journal of biomechanics 33 (12), 1711–1715.

[48] Warner, M., Chappell, P., Stokes, M., 2012. Measuring scapular kinematics during arm lowering using the acromion marker cluster. Human movement science 31 (2), 386–396.

[49] Winter, D. A., 2009. Biomechanics and motor control of human movement. John Wiley & Sons.

[50] Woltring, H., Huiskes, R., De Lange, A., Veldpaus, F., 1985. Finite centroid and helical axis estimation from noisy landmark measurements in the study of human joint kinematics. Journal of biomechanics 18 (5), 379–389.

[51] Wu, G., Van der Helm, F. C., Veeger, H. D., Makhsous, M., Van Roy, P., Anglin, C., Nagels, J., Karduna, A. R., McQuade, K., Wang, X., et al., 2005. Isb recommendation on definitions of joint coordinate systems of various joints for the reporting of human joint motion—part ii: shoulder, elbow, wrist and hand. Journal of biomechanics 38 (5), 981–992.

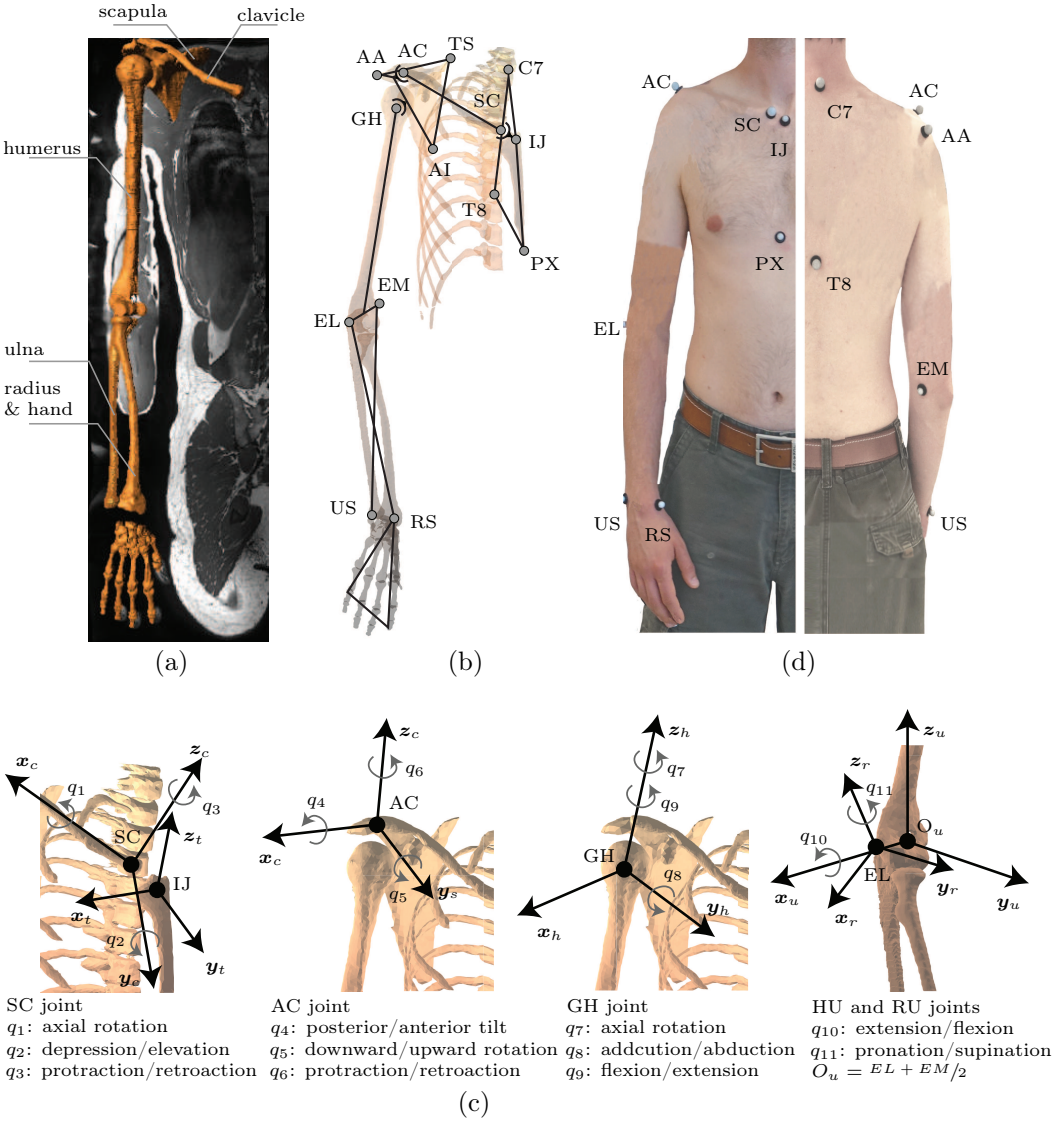

Figure 1: (a) Subject's MRI was used to develop the kinematic model. (b) Fourteen landmarks are considered. (c) Eleven generalized coordinates are considered ($\boldsymbol{q} = [q1 \ \ldots \ q_{11}]^T$). (d) VICON videogrammetry is used to track eleven skin-fixed markers.

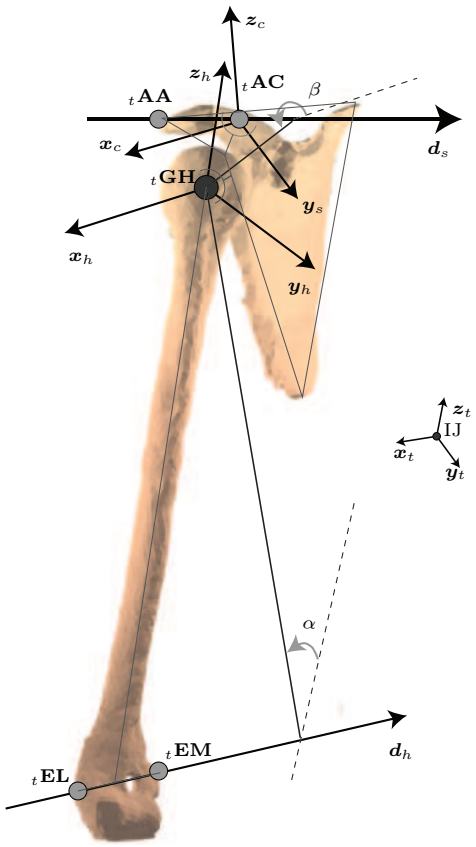

Figure 2: GH belongs to both humerus and scapula. The estimated ${}_t\mathbf{GH}$ lies on the intersection of two line segments in planes perpendicular to $\boldsymbol{d}_h$ and $\boldsymbol{d}_s$. These two line segments form two angles (α and β) with respect to reference axes that can be found by solving Eq. 3.

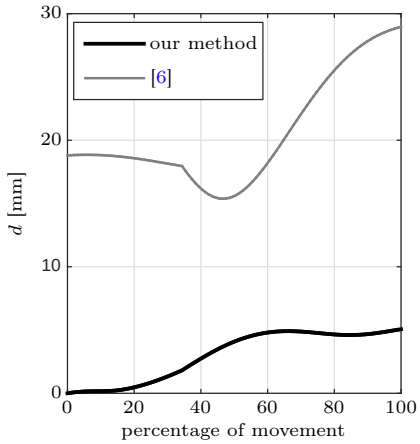

Figure 3: Method accuracy, distance d of the estimated GH to its reference position during arm flexion. The model developed in [6] was directly applied in this study to the same pseudo-measurements, and the corresponding results were presented.

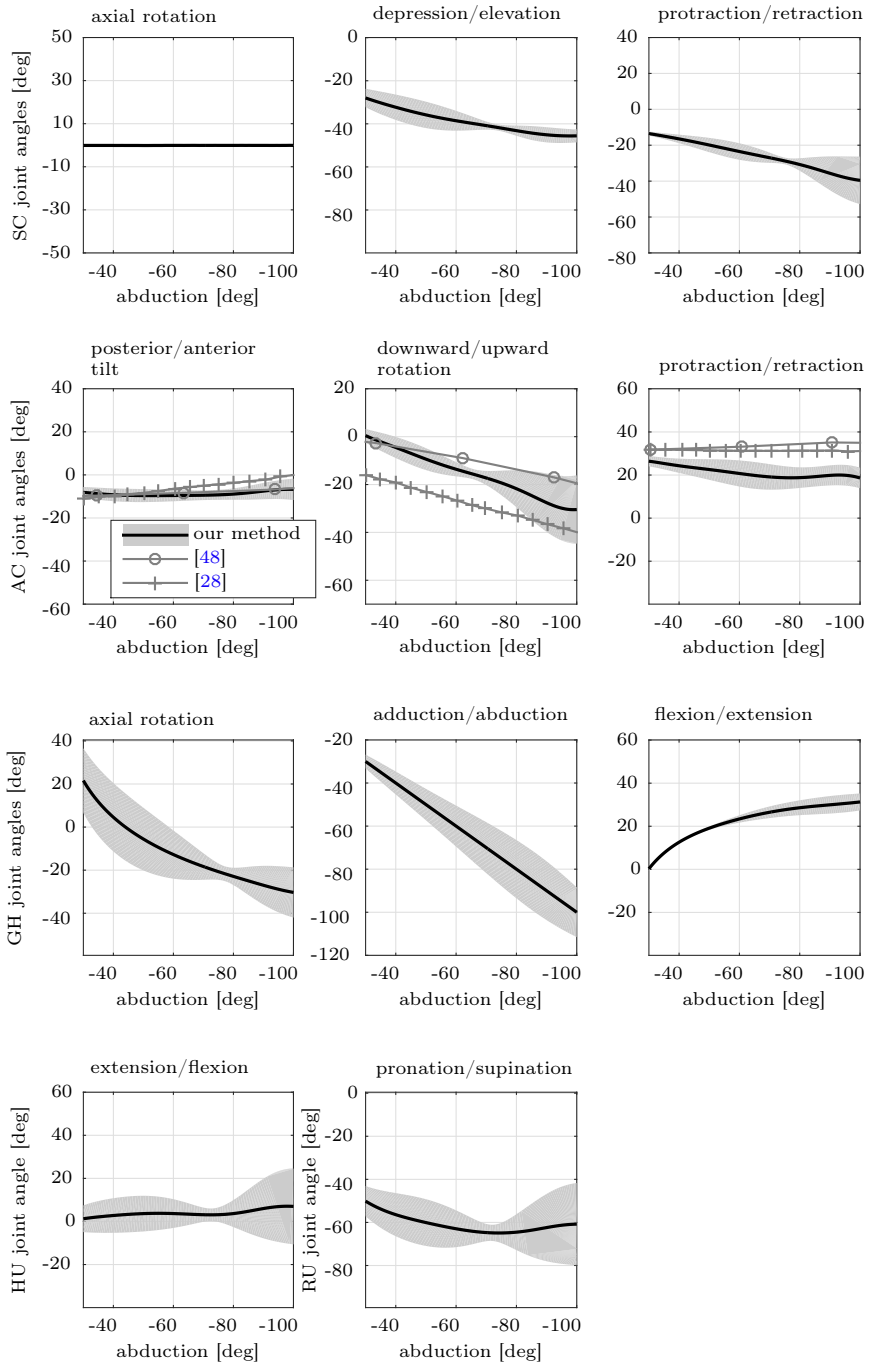

Figure 4: Motion reconstruction, the measured abduction motion was reconstructed in terms of 11 joint angles. The angles sensitivities to $\pm 1\sigma$ landmarks variations were presented as the shaded area. The AC joint angles measured *in vivo* by [28, 48] were also presented, given the importance of the scapula kinematics.